

Efficient and accurate extraction of *in vivo* calcium signals from microendoscopic video data

Pengcheng Zhou
Carnegie Mellon University
pengchez@andrew.cmu.edu

Shanna L. Resendez, Garret D. Stuber
University of North Carolina, Chapel Hill
{shanna_resendez, gstuber}@med.unc.edu

Robert E. Kass
Carnegie Mellon University
kass@stat.cmu.edu

Liam Paninski
Columbia University
liam@stat.columbia.edu

Abstract

In vivo calcium imaging through microscopes has enabled deep brain imaging of previously inaccessible neuronal populations within the brains of freely moving subjects. However, microendoscopic data suffer from high levels of background fluorescence as well as an increased potential for overlapping neuronal signals. Previous methods fail in identifying neurons and demixing their temporal activity because the cellular signals are often submerged in the large fluctuating background. Here we develop an efficient method to extract cellular signals with minimal influence from the background. We model the background with two realistic components: (1) one models the constant baseline and slow trends of each pixel, and (2) the other models the fast fluctuations from out-of-focus signals and is therefore constrained to have low spatial-frequency structure. This decomposition avoids cellular signals being absorbed into the background term. After subtracting the background approximated with this model, we use Constrained Nonnegative Matrix Factorization (CNMF, Pnevmatikakis et al. (2016)) to better demix neural signals and get their denoised and deconvolved temporal activity. We validate our method on simulated and experimental data, where it shows fast, reliable, and high quality signal extraction under a wide variety of imaging parameters.

1 Introduction

Monitoring the activity of large-scale neuronal ensembles during complex behavioral states is fundamental to neuroscience research. Continued advances in optical imaging technology are greatly expanding the number and depth of neuronal populations that can be visualized. Specifically, in vivo calcium imaging through microendoscopic lenses and the development of miniaturized microscopes have enabled deep brain imaging of previously inaccessible neuronal populations of freely moving mice (Flusberg et al. (2008); Ghosh et al. (2011); Ziv and Ghosh (2015)). While these techniques have been widely used by neuroscientists, automatic methods for extracting cellular signals from this data are currently limited and suboptimal. The desired method should be able to (1) identify spatial footprints of all neurons, (2) denoise, demix and deconvolve the temporal signals (Pnevmatikakis et al. (2016)).

Figure 1A is an example frame from microendoscopic data, where the weak neuronal signals are submerged in the large background (the raw video data can be watched here https://www.dropbox.com/s/bszxhcydowntwpr/example_movie.avi?dl=0). For illustrative purposes, we draw two ROIs in the optical field and compute their mean fluorescence intensities (Figure 1C,D). The red ROI overlaps with one neuron and the green ROI only has the background

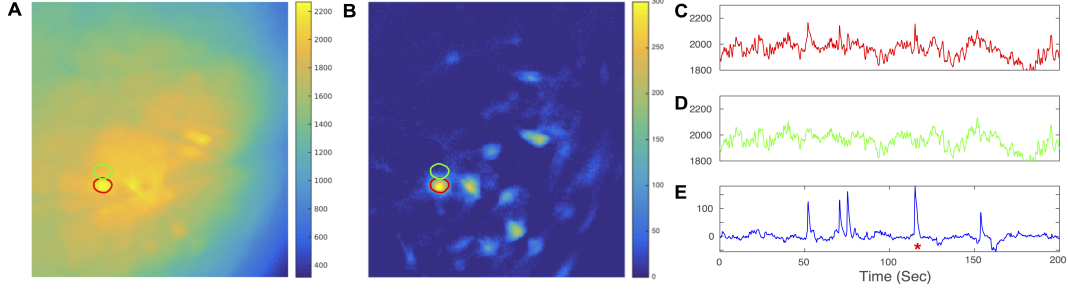


Figure 1: The background of microendoscopic data is strong and has rapid fluctuations. A, one frame of the video data and two selected ROIs corresponding to a neuron (red) and a background area (green). B, same frame as A, but the background has been subtracted using our proposed method. C, average fluorescence intensity within the red ROI. D, average fluorescence intensity within the green ROI. E, difference between C and D. The red star indicates the time-step of the frame in A.

(Figure 1B). Thus the fluorescence in the red ROI (Figure 1C) is a superposition of the background and the neuron’s temporal activity, whereas the green (Figure 1D) provides an estimation of the background signal. By subtracting these two traces, we are able to roughly estimate the temporal activity of the neuron within the red ROI (Figure 1E). From this example, we can see that the background is an order of magnitude larger than the neural activity and its fluctuations are as fast as neuronal calcium transients. These features make it difficult to detect and demix cellular signals automatically from the raw video.

1.1 Previous work

Our work is based on a matrix factorization approach, which can simultaneously segment cells and estimate changes in fluorescence in the temporal domain. This approach stems from the observation that spatiotemporal calcium activity can be approximated as product of two matrices: a spatial matrix that encodes the location of each neuron and a temporal matrix that characterizes the calcium concentration evolution for each neuron. It has several variations with different constraints, such as Independent Component Analysis (PCA-ICA, Mukamel et al. (2009)), Nonnegative Matrix Factorization (NMF, Maruyama et al. (2014)), sparse space-time deconvolution (SSTD, Andilla and Hamprecht (2014)) and Constrained Nonnegative Matrix Factorization (CNMF, Pnevmatikakis et al. (2016)). In particular, PCA-ICA seeks spatiotemporal components that have reduced dependence. It is an inherently linear demixing method and can fail in the case when the neural components exhibit significant spatial overlaps (Pnevmatikakis et al. (2016)). Nonlinear methods like NMF, SSTD and CNMF can deal with overlapping neural sources more effectively, and often outperform PCA-ICA. The main applications of these nonlinear methods are 2-photon or light-sheet imaging data, where the background is weak and has simple spatiotemporally separable structure. They usually model the background with a rank-1 nonnegative matrix.

However, applying these nonlinear matrix factorization methods to the microendoscopic data faces two problems: (1) the background term is not well modeled by rank-1 NMF and its large residual could contaminate the extracted neuronal signals; (2) the procedures of initializing the model parameters, especially spatial and temporal components of neurons, in these models do not work well because the strong and noisy background mixes with the weak neural signals. Since the optimization problem in these methods are non-convex, without good initialization, it may lead to low-quality results or require excessive time for convergent results.

1.2 Contributions

In this paper, we extend the CNMF framework (Pnevmatikakis et al. (2016)) to address strong fluctuations in background fluorescence, and make it applicable to microendoscopic data. Like the proposed CNMF in Pnevmatikakis et al. (2016), our extended CNMF for microEndoscopic data (CNMF-E) also has the capability of identifying neurons with low signal-to-noise ratio (SNR) and simultaneously denoising, deconvolving and demixing large-scale microendoscopic data. To accomplish this: (1) we replace the rank-1 NMF approximation of the background with a more

sophisticated approximation, which can better account the complex background and avoid absorbing cellular signals, and (2) we develop an efficient initialization procedure to extract neural activities with minimal influence from the background.

The structure of the paper is as follows. In Section 2 we briefly review the CNMF model and describe our modifications to the model. In Section 3, we develop our specialized model fitting procedure. In Section 4 we validate our new proposed CNMF-E on simulated and experimental data, and we also compare it with the widely used PCA-ICA method (Mukamel et al. (2009)).

Notation A matrix $Y \in \mathbb{R}^{d \times T}$ represents the spatiotemporal activity of d pixels in T frames. The column vector $Y(t)$ is the observation of the whole frame in time-step t . We use $\mathbf{x} \in \mathbb{R}^2$ to refer the spatial location of one pixel, thus $y(\mathbf{x}, t)$ is the fluorescence intensity in t -th frame at location \mathbf{x} . For a column vector $\mathbf{a} \in \mathbb{R}^d$ encoding the spatial information of d pixels, $a(\mathbf{x})$ indicates the value of \mathbf{a} at pixel \mathbf{x} .

2 Model description

The video data we have are observations from the optical field for a total number of T frames. The recorded data can be represented by a matrix $Y \in \mathbb{R}_+^{d \times T}$, where d is the number of pixels in the field. Each neuron is characterized by its spatial ‘footprint’ vector $\mathbf{a}_i \in \mathbb{R}_+^d$ and ‘calcium activity’ $\mathbf{c}_i \in \mathbb{R}_+^T$. Here both \mathbf{a}_i and \mathbf{c}_i are forced to be nonnegative because of their physical interpretations. Given $\mathbf{a}_i, \mathbf{c}_i$ of one neuron, its spatiotemporal activity is represented as $\mathbf{a}_i \cdot \mathbf{c}_i^T$. The background activity is represented by a matrix $B \in \mathbb{R}_+^{d \times T}$. Suppose the field contains a total number of K neurons, then the observation is a superposition of all neurons’ spatiotemporal activity, time-varying background and additive noise:

$$Y = \sum_{i=1}^K \mathbf{a}_i \cdot \mathbf{c}_i^T + B + E = A \cdot C + B + E, \quad (1)$$

where $A = [\mathbf{a}_1, \dots, \mathbf{a}_K]$, $C = [\mathbf{c}_1, \dots, \mathbf{c}_K]^T$. The noise term $E \in \mathbb{R}^{d \times T}$ is assumed to be Gaussian and $E(t) \sim \mathcal{N}(\mathbf{0}, \Sigma)$. Σ is a diagonal matrix indicating that the noise is spatially and temporally uncorrelated.

Pnevmatikakis et al. (2016) also explicitly model the calcium dynamics \mathbf{c}_i with a stable autoregressive process (AR) of order p ,

$$c_i(t) = \sum_{j=1}^p \gamma_j^{(i)} c_i(t-j) + s_i(t), \quad (2)$$

where $s_i(t) \geq 0$ is the number of spikes that neuron fired at the t -th frame and it is sparse in the neural systems. The AR coefficients $\{\gamma_j^{(i)}\}$ are different for each neuron and they are estimated from the data.

Estimating the model parameters A, C in model (1)(2) can give us all neurons’ spatial footprints and their deconvolved temporal activities. To fit the model, we also have to constrain the background term to have simplified structure, otherwise letting $B = Y$ leads to the least reconstruction error. This framework is general and we use it in our new method as well. Compared with the proposed implementation in Pnevmatikakis et al. (2016), our method models the background term differently.

In the work of Pnevmatikakis et al. (2016), they model the background with a rank-1 nonnegative matrix $\mathbf{b} \cdot \mathbf{f}^T$, where $\mathbf{b} \in \mathbb{R}_+^d$ and $\mathbf{f} \in \mathbb{R}_+^T$ encode the background spatial and temporal structure respectively. This is a good assumption for two-photon or light-sheet imaging data, but the background in microendoscopic data requires a more complex model. We also have to avoid the increased complexity from absorbing cellular signals into the background. Thus the ideal model should explicitly model the background features that are distinct from neurons of interest. Here we include two main features of the background into the model of B : (1) the temporal component of each pixel has a constant large baseline and some slow trends (See Figure 1D) and (2) background is usually spatially smooth in a larger spatial range compared with neuron size (Figure 1), which means the background of all pixels within a neuron does not have large spatial gradients. This is because the fluctuations in the background reflects the out-of-focus fluorescence and they are significantly blurred. Hence we model the background term as

$$B = B_{trend} + UV, \quad (3)$$

where $B_{trend} \in \mathbb{R}^{d \times T}$ and $U \in \mathbb{R}^{d \times N}$, $V \in \mathbb{R}^{N \times T}$. B_{trend} explains the constant baselines and slow trends for all pixels (Figure 1C) and their temporal dynamics are much slower than calcium indicators. The second term UV models the fast fluctuation in the background and the spatial component U has low spatial-frequency structure. The constraint of U excludes cellular signals from the background term.

3 Model fitting

In this section, we will describe our customized algorithm for fitting the model (1)(2)(3). We frequently use the pixel-wise formulation of model (1) and ignore the noise term:

$$y(\mathbf{x}, t) = \sum_{i=1}^K a_i(\mathbf{x}) \cdot c_i(t) + b(\mathbf{x}, t). \quad (4)$$

Our framework can be summarized into the following steps:

1. Initialize \hat{A}, \hat{C} using the new initialization procedure.
2. Approximate the background \hat{B} using model (3).
3. Update \hat{A}, \hat{C} from data $(Y - \hat{B})$ using constrained alternating matrix factorization.
4. post-process the results automatically or manually: delete neurons, pick the missed neurons from the residuals, and merge neurons with high temporal correlations.
5. Repeat steps 2, 3, 4 until the results are biologically meaningful.

Our techniques differ from Pnevmatikakis et al. (2016) in the following aspects: (1) the initialization step for A and C here requires careful considerations of the background contaminations and our approach is totally new. (2) instead of updating the background term iteratively, we update the background independently in different iterations and the rank of the background model can be modified in each iteration. As a result, our algorithm has a better control of the residual levels in background.

In the followings, we mainly describe our novel initialization step and briefly summarize the procedure of fitting the background term. As for steps (3-5) and discussions for scalability issue, we put them in the supplementary materials (Section 6.5 and 6.7).

3.1 Initialization of A, C

Here we develop a robust procedure for initializing A and C without estimation of the background. This procedure utilizes the spatial smoothness feature in the background and removes it by spatial high-pass filtering of the raw data. We estimate the temporal component of one neuron c_i from spatially filtered data and then use it to extract the corresponding spatial footprint a_i from the raw data. In the step of estimating a_i , we re-order all frames to make nearby frames share the similar local background levels and then take the temporal differencing to remove the background signals temporally. After that, we can use regression to get a_i . Repeating this process can initialize the required number of neurons. The whole procedure is schematically illustrated in Figure 2 and described in Algorithm 1 in the supplementary materials.

3.1.1 Spatially high-pass filter the raw data

The spatial smoothness assumption of the background leads to

$$b(\mathbf{x}, t) \approx b(\mathbf{x}', t) \text{ if } \|\mathbf{x} - \mathbf{x}'\| \leq r, \quad (5)$$

i.e., within the spatial range of a cell body, the background is spatially invariant. Based on this assumption, we use $\tilde{h}(\mathbf{x})$ to filter the raw data $y(\mathbf{x}, t)$, and $\tilde{h}(\mathbf{x})$ is defined as

$$\tilde{h}(\mathbf{x}) = \begin{cases} h(\mathbf{x}) - \int_{\Omega} h(\mathbf{x}) d\mathbf{x} / \int_{\Omega} 1 \cdot d\mathbf{x} & \text{for } \mathbf{x} \in \Omega \\ 0 & \text{else where} \end{cases} \quad (6)$$

where $h(\mathbf{x}) = \exp(-\frac{\|\mathbf{x}\|^2}{2\sigma^2})$, $\Omega = \{\mathbf{x} | \|\mathbf{x}\| \leq r\}$. $h(\mathbf{x})$ is a Gaussian kernel with width σ and r is the the average size of the neurons. $\tilde{h}(\mathbf{x})$ is a template matching filter to detect spatial structures

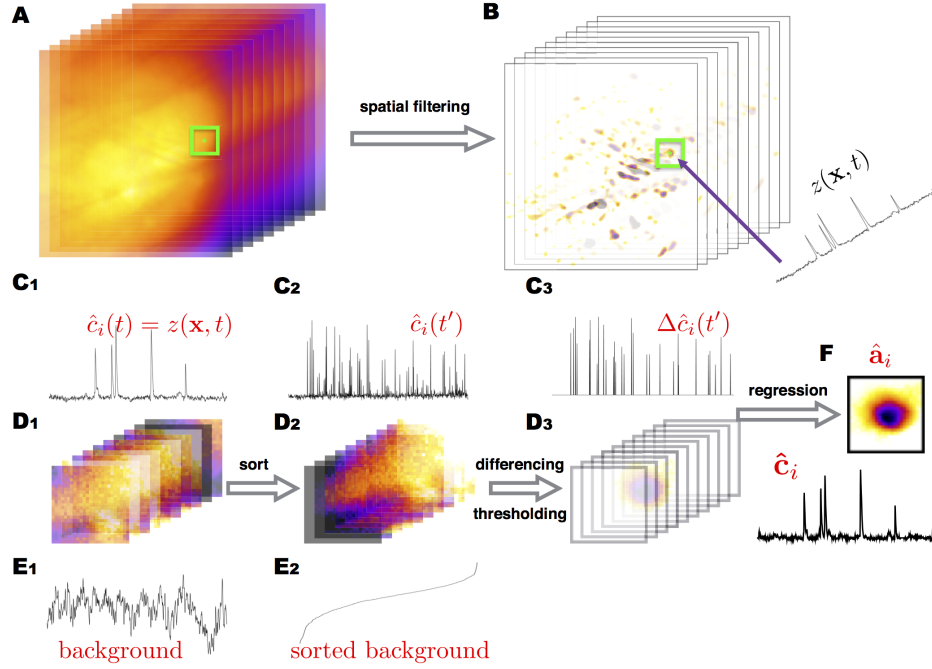


Figure 2: Illustration of the initialization procedure. A, raw data. B, spatially high-pass filtered data and the temporal trace of one seed pixel (green dot). C₁, the initialized temporal activity of one neuron. D₁, raw data of the cropped small window (green square in A and B). E₁, the estimated time-varying local backgrounds in the small cropped window. C₂, D₂ and E₂ are the re-ordered version of C₁, D₁ and E₁. C₃ is the temporal differencing of C₂ and the result has been thresholded with its 2 standard deviation. Similarly, D₃ is differencing result of D₂. F, the initialized spatial and temporal components of the neuron.

with similar shapes and sizes. For flat structures in the small regions, like background, filtering them with $\tilde{h}(\mathbf{x})$ get results close to 0. Thus in the filtered data $z(\mathbf{x}, t) = \tilde{h}(\mathbf{x}) * y(\mathbf{x}, t)$, the background $b(x, t)$ has been roughly removed and $z(\mathbf{x}, t)$ is mainly composed of cellular signals (Figure 2B). More interestingly, the calcium concentrations of most neurons can be directly approximated by the temporal traces of some pixels in $z(\mathbf{x}, t)$. (Figure 2C₁, see Section 6.1 in supplementary materials for derivation). We call these pixels seed pixels because we can use them to initialize neurons.

3.1.2 Greedy initialization of all neurons

We initialize neurons with a greedy algorithm. In each iteration, we find one seed pixel \mathbf{x}^* (See supplementary materials Section 6.2 for details of how to detect seed pixels) and initialize its spatial footprint $\hat{\mathbf{a}}(\mathbf{x})$ and temporal course $\hat{\mathbf{c}}_i$. Then we subtract $\hat{\mathbf{a}}_i \hat{\mathbf{c}}_i^T$ from the raw video data, find the next seed pixel and repeat the initialization procedure until specified number of neurons have been initialized or no more seed pixels exist.

Given a seed pixel \mathbf{x}^* , we can initialize the neuron's temporal component as $\hat{\mathbf{c}}_i(t) = z(\mathbf{x}^*, t)$ (Figure 2C₁). This approximation is usually good, and here we propose an efficient method to extract its spatial component \mathbf{a}_i from the raw data Y .

we first crop the optical field with a square centered at \mathbf{x}^* and the square size is twice larger than the average neuron size r (Figure 2D₁). Since cell bodies have localized structure, the spatial shape of the expected neuron is completely covered by this square. Then we approximate the local background level in this cropped area $\hat{y}_b(t)$ using the median of the fluorescence intensities on the square boundary

(Figure 2E₁). By sorting all frames in an order of $\{u_k\}$ such that $\hat{y}_b(u_1) \leq \hat{y}_b(u_2) \leq \dots \leq \hat{y}_b(u_T)$ (Figure 2C₂D₂E₂), nearby frames have the minimal differences (≈ 0) in the background term. Hence the differencing of the sorted video data is

$$\Delta y(\mathbf{x}, u_k) = y(\mathbf{x}, u_{k+1}) - y(\mathbf{x}, u_k) \approx a_i(\mathbf{x}) \cdot \Delta c_i(u_k) + \sum_{j \neq i}^K a_j(\mathbf{x}) \cdot \Delta c_j(u_k). \quad (7)$$

We already have $\hat{c}_i(t)$, so we can initialize \mathbf{a}_i by regressing $\Delta y(\mathbf{x}, u_i)$ on $\Delta c_i(u_i)$ (Figure 2C₃D₃). Empirically we found that thresholding Δc_i achieves better results. After we get $\hat{\mathbf{a}}_i$ (Figure 2F), we can reestimate $\hat{c}_i(t)$ using a simple formula:

$$\hat{c}_i(t) = \max\{0, \frac{(\hat{\mathbf{a}}_i - \bar{\mathbf{a}}_i)^T \cdot Y(t)}{(\hat{\mathbf{a}}_i - \bar{\mathbf{a}}_i)^T \cdot \hat{\mathbf{a}}_i}\}, \quad (8)$$

where $\bar{\mathbf{a}}$ is a vector replacing all nonzero pixels of $\hat{\mathbf{a}}_i$ with the mean of those nonzero pixels. By running this initialization procedure iteratively, we can extract almost all neurons.

3.2 Approximate the background using model (3)

After we get \hat{A} and \hat{C} , $(Y - \hat{A}\hat{C})$ is mainly the background component and we will approximate it with a matrix described in Eq. (3). First we use a spline basis with low temporal dynamics to approximate the first term \hat{B}_{trend} (baseline + slow trend), then we factorize the residual $Y - \hat{A}\hat{C} - \hat{B}_{trend}$ with UV . By constraining U with high spatial smoothness, we can avoid cellular signals being absorbed into the background. We use Singular Value Decomposition (SVD) together with low-pass filtering of the estimated spatial components to estimate \hat{U} and \hat{V} . (See Supplementary materials 6.4 for details).

4 Results

PCA-ICA (Mukamel et al. (2009)) is the most widely used automatic methods for analyzing microendoscopic data (Resendez et al. (2016)). It seeks spatially and temporally independent components as individual neurons. In this section We compared our CNMF-E with PCA-ICA method using simulated and experimental data.

4.1 Simulated data

We simulated 200 neurons' activity in the optical field (256×256 pixels) for 3000 frames (20 Hz). To ensure that the background had similar features as real data, we utilized the background extracted from our experimental data as the background in our simulation. We also add i.i.d. Gaussian noise to our model (The simulated video data can be found here https://www.dropbox.com/s/i6op3btktwnoanw/simulated_data.avi?dl=0).

After removing all false positives, PCA-ICA detected 116 neurons and our CNMF-E method found 199 neurons of the 200 neurons. Most neurons detected by PCA-ICA did not have localized structures and multiple neurons were combined together (See Supplementary Figure 5). We superimposed the contours of all extracted neurons together on top of the locations of simulated neurons. PCA-ICA-based segmentation failed to identify a large proportion of the neurons in this dataset, whereas nearly every neuron was identified by the CNMF-E approach (Figure 3CD). We matched each simulated neuron with a neuron among all the extracted neurons by selecting the one most correlated with the simulated neuron temporally. For a pair of matched neuron, they should have both high temporal and spatial correlations in the perfect case, i.e., the real cellular signal is extracted from the data with high fidelity. We displayed spatial and temporal correlations of all simulated neurons with their matched neurons detected by two approaches (Figure 3BD). A total number of 199 simulated neurons were accurately recovered by our CNMF-E method (Figure 3D). While for PCA-ICA, a large proportion of the matched neurons have low spatial and temporal correlations (Figure 3) indicating failures in recovering real neurons' signals.

We also display 4 tightly clustered neurons in the simulated data (Figure 3E) to demonstrate that our CNMF-E approach can accurately detect and demix their activity (Figure 3G). The spatiotemporal similarity between the 4 neurons segmented with CNMF-E (Figure 3G) and ground truth (Figure 3E)

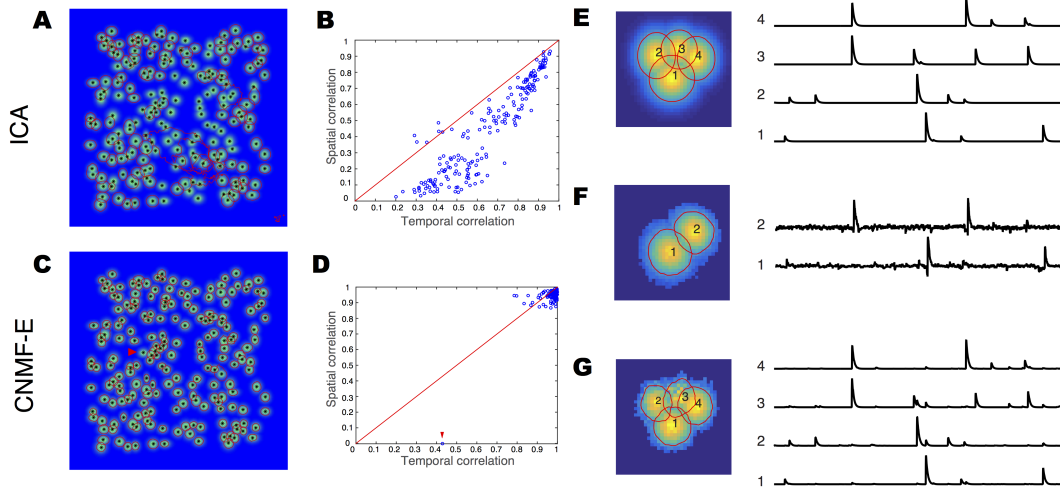


Figure 3: Comparisons of PCA-ICA and CNMF-E in recovering simulated neural signals. A, contours of neurons extracted with PCA-ICA method and neurons’ true spatial footprints. black asterisks indicate the centers of all real neurons. B, temporal and spatial correlations between each ground truth neuron and its matched neurons in the extracted neuron pool. CD, same as AB, but for CNMF-E method. Red triangles indicate the missed neuron. E, ground truth of 4 close neurons and their calcium traces. F, detected neurons and calcium traces by PCA-ICA method. G, detected neurons and calcium traces by CNMF-E.

indicates a good performance in extracting the neural activity. In contrast, PCA-ICA based detection can only detect two neurons and the calcium traces have high level of noise. The reason is that PCA-ICA merges multiple neurons together spatially and distorts the calcium traces in the temporal domain. Furthermore, the distorted calcium traces reduces the number of detected neurons.

4.2 Experimental data

The data used here was collected from the prefrontal cortex (PFC) of a freely moving mouse. The frame rate is 15 Hz. The raw image (Figure 4A) is blurry and it is difficult to visually detect any neurons. Its local correlation image (Smith and Häusser (2010)) of the raw data is approximately uniform 1 (Figure 4C), which means neighboring pixels share strong background fluctuations. Here we removed the background by spatially filtering the raw data with $\tilde{h}(x)$ and then calculated local correlation image using Eq. (14) in supplementary materials. Figure 4D clearly shows the locations of all neurons. Applying our proposed CNMF-E method is able to detect 226 neurons from the raw data. Their contours are depicted on top the the correlation image and we can see that our method efficiently identifies neurons in the optical field (Figure 4D).

After subtracting the extracted background from the raw data, neural activity is visualized more effectively (Figure 4B). The quality of this background correction on the raw data is important for extracting neural signals and demixing neurons. In the supplementary video (<https://www.dropbox.com/s/e6pdubwnsqoclt/exp.avi?dl=0>), we showed the raw video, extracted background video, background corrected video and reconstructed cellular activity $A \cdot C$. From the video, we can see that CNMF-E reliably extracted the weak cellular signals from the rapidly fluctuating background.

We choose three neighboring neurons within a small field to show the performance of our method. In Figure 4E, we showed their ROIs and the local correlation image. The mean fluorescence traces within each ROI are too noisy to infer any calcium events. Both PCA-ICA and CNMF-E isolated these three neurons and extracted the spiking signals, but the traces extracted with the PCA-ICA have higher levels of noise. Further, note that traces extracted with PCA-ICA have large artifactual negative peaks. CNMF-E does not have this problem due to the nonnegative requirements. In the shaded region of Figure 4F, we demonstrate potential crosstalk between two neurons, that is avoided by CNMF-E but not PCA-ICA based segmentation (watch video here

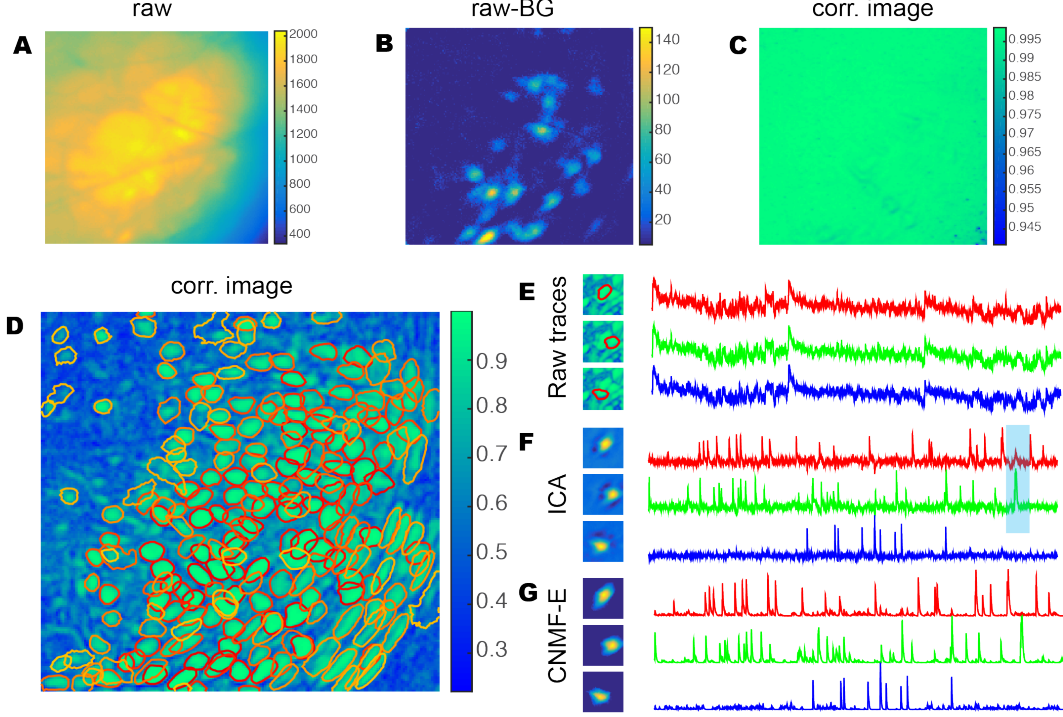


Figure 4: Examples of extracting cellular signals from experimental data. A, an example frame from the raw data. B, background corrected result of the image in A. C, local correlation image calculated using the raw data. D, contours of all 226 detected neurons and the correlation image calculated using our CNMF-E method (See Eq. (14) in supplementary materials). E, mean fluorescence traces from three ROIs. F, Extracted spatial/temporal components of three neurons using PCA-ICA method. G, results using our CNMF-E method.

https://www.dropbox.com/s/loxsniw19ugxdw/neuron_movie_trace.avi?dl=0. The temporal traces in the video are extracted from CNMF-E).

5 Conclusion

In this paper, we proposed an efficient method for extracting cellular signals from microendoscopic data; such methods are in very high demand in the neuroscience community. The analysis of this video data is the first stage of processing in many experiments, so the quality of source extraction in this step highly influences the scientific conclusions drawn in downstream analysis. As shown in Figure 3 and 4, our method shows credible performances in recovering the real neuronal signals and outperforms the previous standard PCA-ICA method. Thus the methods introduced here (which we plan to release as open source software) will be a powerful and important tool for the neuroscience community.

Acknowledgments

Funding for this research was provided by NIH 2R01MH064537 (P.Z., R.K.), NIH R90DA023426 (P.Z.), National Institute of Child Health NICHD and Human Development HD079124 (G.S.), NICHD Grant T32 HD040127 (S.R.), Simons Research Foundation (G.S.), Simons Foundation Global Brain Research Awards 325171, 365002, ARO MURI W911NF-12-1-0594, DARPA N66001-15-C-4032 (SIMPLEX), and a Google Faculty Research award (L.P.); in addition, this work was supported by the Intelligence Advanced Research Projects Activity (IARPA) via Department of Interior/ Interior Business Center (DoI/IBC) contract number D16PC00003 (L.P.), D16PC00007 (P.Z.). The U.S. Government is authorized to reproduce and distribute reprints for Governmental purposes notwithstanding any copyright annotation thereon. Disclaimer: The views and conclusions

contained herein are those of the authors and should not be interpreted as necessarily representing the official policies or endorsements, either expressed or implied, of IARPA, DoI/IBC, or the U.S. Government.

References

- Ferran Diego Andilla and Fred a. Hamprecht. Sparse Space-Time Deconvolution for Calcium Image Analysis. *Advances in Neural Information Processing Systems*, pages 64–72, 2014.
- Andrzej Cichocki, Rafal Zdunek, and Shun-ichi Amari. Hierarchical ALS Algorithms for Nonnegative Matrix and 3D Tensor Factorization. *Independent Component Analysis and Signal Separation*, 4666(1):169–176, 2007.
- Benjamin A Flusberg, Axel Nimmerjahn, Eric D Cocker, Eran A Mukamel, Robert P J Barretto, Tony H Ko, Laurie D Burns, Juergen C Jung, and Mark J Schnitzer. High-speed, miniaturized fluorescence microscopy in freely moving mice. *Nature methods*, 5(11):935–8, 2008.
- Johannes Friedrich, Daniel Soudry, Yu Mu, Jeremy Freeman, Misha Ahrens, and Liam Paninski. Fast Constrained Non-negative Matrix Factorization for Whole-Brain Calcium Imaging Data. In *Conference on Neural Information Processing Systems*, 2015.
- Kunal K Ghosh, Laurie D Burns, Eric D Cocker, Axel Nimmerjahn, Yaniv Ziv, Abbas El Gamal, and Mark J Schnitzer. Miniaturized integration of a fluorescence microscope. *Nature Methods*, 8(10): 871–878, 2011.
- Ryuichi Maruyama, Kazuma Maeda, Hajime Moroda, Ichiro Kato, Masashi Inoue, Hiroyoshi Miyakawa, and Toru Aonishi. Detecting cells using non-negative matrix factorization on calcium imaging data. *Neural Networks*, 55:11–19, 2014.
- Eran A. Mukamel, Axel Nimmerjahn, and Mark J. Schnitzer. Automated Analysis of Cellular Signals from Large-Scale Calcium Imaging Data. *Neuron*, 63(6):747–760, 2009.
- Eftychios A Pnevmatikakis, Daniel Soudry, Yuanjun Gao, Timothy A Machado, Josh Merel, David Pfau, Thomas Reardon, Yu Mu, Clay Lacefield, Weijian Yang, Misha Ahrens, Randy Bruno, Thomas M Jessell, Darcy S Peterka, Rafael Yuste, and Liam Paninski. Simultaneous Denoising, Deconvolution, and Demixing of Calcium Imaging Data. *Neuron*, 89(2):285–299, 2016.
- Shanna L Resendez, Josh H Jennings, Randall L Ung, Vijay Mohan K Namboodiri, Zhe Charles Zhou, James M Otis, Hiroshi Nomura, Jenna A McHenry, Oksana Kosyk, and Garret D Stuber. Visualization of cortical, subcortical and deep brain neural circuit dynamics during naturalistic mammalian behavior with head-mounted microscopes and chronically implanted lenses. *Nature Protocols*, 11(3):566–597, 2016.
- Spencer L Smith and Michael Häusser. Parallel processing of visual space by neighboring neurons in mouse visual cortex. *Nature Neuroscience*, 13(9):1144–1149, 2010.
- Yaniv Ziv and Kunal K Ghosh. Miniature microscopes for large-scale imaging of neuronal activity in freely behaving rodents. *Current Opinion in Neurobiology*, 32:141–147, 2015.

6 Supplementary materials

6.1 Approximate $c_i(t)$ from the spatially filtered data

Since

$$\tilde{h}(\mathbf{x}) * b(\mathbf{x}, t) = \int_{\Omega} \tilde{h}(\mathbf{x}_1) \cdot b(\mathbf{x} - \mathbf{x}_1, t) d\mathbf{x}_1 \quad (9)$$

$$\approx \int_{\Omega} \tilde{h}(\mathbf{x}_1) \cdot b(\mathbf{x}, t) d\mathbf{x}_1 \quad (10)$$

$$= b(\mathbf{x}, t) \cdot \int_{\Omega} \tilde{h}(\mathbf{x}_1) d\mathbf{x}_1 = 0, \quad (11)$$

Algorithm 1: Initialization procedure for extracting spatial and temporal components of the neurons

Input: data $Y \in \mathbb{R}_+^{d \times T}$, maximum number of neurons K , average neuron size r , width of 2D Gaussian kernel σ , minimum local correlation c_{\min} , minimum peak-to-noise ratio α_{\min}

Output: A, C

```

1 begin
2   Create the kernel of the spatial filter,  $\tilde{h} \leftarrow \text{kernel}(r, \sigma)$  (See Eq. 6)
3   Filter the raw data  $Y$  with the kernel  $\tilde{h}$ ,  $Z \leftarrow \tilde{h} * Y \in \mathbb{R}^{d \times T}$ 
4   Compute the local correlation image,  $L \leftarrow \text{LocalCorrelation}(Z) \in \mathbb{R}^{d \times 1}$ 
5   Compute the peak-to-noise ratio (PNR),  $P \leftarrow \text{PNR}(Z)$  (See Supplementary Materials 6.2)
6   Define  $k = 0$ 
7   while  $k \leq K$  do
8     Find one seed pixel  $x^* \leftarrow \underset{\{x | P(x) \geq \alpha_{\min}, L(x) \geq c_{\min}\}}{\text{argmax}} P(x) \cdot L(x)$ 
9     if  $x^*$  is not empty then
10        $k \leftarrow k + 1$ 
11     else
12       Break
13     end
14     Initialize  $\mathbf{c}_k \leftarrow Z(x^*, :)^T$ 
15     Define  $Y_k \in \mathbb{R}^{(2r+1)^2 \times T}$  to be the raw data of all pixels within the  $(2r+1) \times (2r+1)$  window
        centered at  $x^*$ 
16     Estimate the background level at each frame,  $y_b(t) \leftarrow \text{median}(Y_k(x, t))$ , where  $xs$  are on the
        boundary of the cropped window.
17     Sort  $y_b(t)$  in ascending order,  $seq \leftarrow \text{sorting sequence}$ 
18     Order all frames of  $Y_k$  and  $\mathbf{c}_k$  in the sequence of  $seq$ ,  $Y'_k \leftarrow Y_k(:, seq)$  and  $\mathbf{c}'_k \leftarrow \mathbf{c}_k(seq)$ 
19     Compute the differencing of re-ordered data  $Y'_k$ ,  $\Delta Y'_k(t) \leftarrow Y'_k(t+1) - Y'_k(t)$ 
20     Compute the differencing of re-ordered data  $\mathbf{c}'_k$ ,  $\Delta \mathbf{c}'_k(t) \leftarrow \mathbf{c}'_k(t+1) - \mathbf{c}'_k(t)$ 
21     Threshold  $\Delta \mathbf{c}'_k(t)$  by its 2 standard deviation.
22     Initialize the spatial component  $\mathbf{a}_k \leftarrow \underset{\mathbf{a} \geq 0}{\text{argmax}} \|\Delta Y'_k - \mathbf{a} \cdot \Delta \mathbf{c}'_k\|_2^2$ 
23     Update the temporal component  $\mathbf{c}_k \leftarrow \max\{0, \frac{(\mathbf{a}_k - \bar{\mathbf{a}}_k)^T \cdot Y(t)}{(\mathbf{a}_k - \bar{\mathbf{a}}_k)^T \cdot \mathbf{a}_k}\}$  (See Eq. (8))
24     Peel off the cellular signal of  $k$ th neuron  $Y \leftarrow Y - \mathbf{a}_k \cdot \mathbf{c}_k^T$ 
25     Locally update  $L$  and  $P$ 
26   end
27    $A = [\mathbf{a}_1, \mathbf{a}_2, \dots, \mathbf{a}_K], C = [\mathbf{c}_1, \mathbf{c}_2, \dots, \mathbf{c}_K]^T$ 
28   return
29 end

```

filtering the raw data with $\tilde{h}(\mathbf{x})$ results

$$z(\mathbf{x}, t) = \tilde{h}(\mathbf{x}) * y(\mathbf{x}, t) \approx \sum_{i=1}^K [\tilde{h} * a_i](\mathbf{x}) \cdot c_i(t). \quad (12)$$

For each neuron, there is an area $\Omega_i = \{\mathbf{x} | [\tilde{h} * a_i](\mathbf{x}) > 0\}$. Usually Ω_i corresponds to the central area for a neuron with Gaussian shape. For $\mathbf{x} \in \Omega_i$,

$$z(\mathbf{x}, t) \approx [\tilde{h} * a_i](\mathbf{x}) \cdot c_i(t) + \sum_{j \neq i}^K [\tilde{h} * a_j](\mathbf{x}) \cdot c_j(t). \quad (13)$$

If $[\tilde{h} * a_j](\mathbf{x}) = 0$ for all $j \neq i$, i.e., the i th neuron is well isolated from the others, then $z(\mathbf{x}, t) \propto c_i(t)$. This is a nice feature because we can estimate $c_i(t)$ from $z(\mathbf{x}, t)$ directly. Empirically we found that this condition can be relaxed to $[\tilde{h} * a_j](\mathbf{x}) \leq 0$. When $[\tilde{h} * a_j](\mathbf{x}) < 0$, $z(\mathbf{x}, t)$ has negative spikes from neuron j and we can remove them simply by thresholding $z(\mathbf{x}, t)$ with its median.

Thus for each neuron i , as long as there exist some $\mathbf{x} \in \Omega_i$ and $[\tilde{h} * a_j](\mathbf{x}) \leq 0$ for all $j \neq i$ (small positive values are still tolerable), we can simply approximate its calcium concentration $c_i(t)$ with $z(\mathbf{x}, t)$.

6.2 Detect seed pixels

A seed pixel \mathbf{x} should have two main features: first, $z(\mathbf{x}, t)$ has high peak-to-noise ratio (PNR) because it encodes the calcium concentration $c_i(t)$ of one neuron and usually $c_i(t)$ has large calcium transients; second, seed pixel has high temporal correlations with its neighboring pixels because they are likely to share the same $c_i(t)$. We computed two metrics for each of these two features:

$$P(\mathbf{x}) = \frac{\max(z(\mathbf{x}, t))}{\sigma(\mathbf{x})}, \quad L(\mathbf{x}) = \frac{1}{N} \sum_{\|\mathbf{x}-\mathbf{x}'\| \leq \delta} \langle g(z(\mathbf{x}, t)), g(z(\mathbf{x}', t)) \rangle, \quad (14)$$

where δ (we use $\delta = 1$) determines the range of neighbors and N is the total number of neighboring pixels. $\langle f_1(t), f_2(t) \rangle$ calculates the temporal correlation between two time series $f_1(t)$ and $f_2(t)$. The function $g(\cdot)$ is a pre-processing of $z(\mathbf{x}, t)$ before computing local correlation. In our implementation, we threshold the differencing of $z(\mathbf{x}, t)$ by $\alpha \cdot \sigma(\mathbf{x})$ (e.g., $\alpha = 2$). This is equivalent to a rough detection of calcium transients. It is better than using $z(\mathbf{x}, t)$ directly because it reduces the influence of the background residual, noise and negative spikes from nearby neurons. To avoid unnecessary searches of the seed pixels, we usually set thresholds for both $P(\mathbf{x})$ (e.g., 5) and $L(\mathbf{x})$ (e.g., 0.5). In each iteration of the initialization, we find the pixel with the maximum value of $P(\mathbf{x}) \cdot L(\mathbf{x})$ and set it as a seed pixel. Here we use point-wise product of $P(\mathbf{x})$ and $L(\mathbf{x})$ to emphasize the characteristics of seed pixels. If we successfully initialize one neuron from this seed pixel, the spatiotemporal activity of this initialized neuron $\hat{\mathbf{a}}_i \cdot \hat{\mathbf{c}}_i$ will be peeled off from the residual data (it is Y at the beginning of the initialization). We also have to locally update $P(\mathbf{x})$ and $L(\mathbf{x})$ in the initialized area. Each neuron can only be visited once for initialization. We will stop the initialization procedure until the specified number K reaches or there are no more seed pixels.

6.3 Reestimate $\hat{\mathbf{c}}_i$ given $\hat{\mathbf{a}}_i$

Define $\Theta_i = \{\mathbf{x} | \hat{a}_i(\mathbf{x}) \neq 0\}$ as nonzero pixels of $\hat{\mathbf{a}}_i$ and

$$\bar{a}(\mathbf{x}) = \begin{cases} \int_{\Theta_i} a(\mathbf{x}) d\mathbf{x} / \int_{\Theta_i} 1 \cdot d\mathbf{x} & \text{for } \mathbf{x} \in \Theta_i \\ 0 & \text{else where.} \end{cases} \quad (15)$$

then

$$\hat{\mathbf{a}}_i^T \cdot Y(t) = \hat{\mathbf{a}}_i^T \mathbf{a}_i \cdot c_i(t) + \sum_{j \neq i}^K \hat{\mathbf{a}}_i^T \mathbf{a}_j \cdot c_j(t) + \hat{\mathbf{a}}_i^T \cdot B(t) \quad (16)$$

$$\bar{\mathbf{a}}_i^T \cdot Y(t) = \bar{\mathbf{a}}_i^T \mathbf{a}_i \cdot c_i(t) + \sum_{j \neq i}^K \bar{\mathbf{a}}_i^T \mathbf{a}_j \cdot c_j(t) + \bar{\mathbf{a}}_i^T \cdot B(t) \quad (17)$$

Again, the spatial smoothness of the background term $B(t)$ induces $\hat{\mathbf{a}}_i^T \cdot B(t) = \bar{\mathbf{a}}_i^T \cdot B(t)$. When the overlaps between neurons are not severe, $(\hat{\mathbf{a}}_i - \bar{\mathbf{a}}_i)^T \cdot \mathbf{a}_j \approx 0$. Hence, we have

$$(\hat{\mathbf{a}}_i - \bar{\mathbf{a}}_i)^T \cdot Y(t) \approx (\hat{\mathbf{a}}_i - \bar{\mathbf{a}}_i)^T \cdot \mathbf{a}_i \cdot c_i(t) \quad \Rightarrow \quad c_j(t) \approx \max\{0, \frac{(\hat{\mathbf{a}}_i - \bar{\mathbf{a}}_i)^T \cdot Y(t)}{(\hat{\mathbf{a}}_i - \bar{\mathbf{a}}_i)^T \cdot \hat{\mathbf{a}}_i}\} \quad (18)$$

6.4 Fit background model

The trends of all pixels are independent and we approximate all trends with B-spline basis X , i.e., $B_{trend} = WX$, where the row vectors of X are cubic B-spline basis given a sequences of knots. By increasing the intervals between knots, we lower the number of basis and constrain the dynamics of $b_{trend}(\mathbf{x}, t)$ to be slow. We usually choose evenly distributed knots over the whole time period with an interval of 100 seconds. This is much larger than dynamics of the calcium indicators (~ 1 seconds). W contains coefficients of each spline basis. It is estimated with regression $W = [(Y - \hat{A}\hat{C})X^T] \cdot [XX^T]^{-1}$.

After we remove the B_{trend} , we move on to approximate the the fast fluctuations $B_{fluc.} = Y - \hat{A}\hat{C} - \hat{W}X$ with low rank- N matrix UV . The Truncated SVD of $B_{fluc.}$ has the globally minimum Frobenious norm of the difference between $B_{fluc.}$ and UV . Here we choose row vectors of \hat{V} be the top N right singular vectors of $B_{fluc.}$ and then $U = B_{fluc.}V$. However, the computed U is not guaranteed to have low spatial frequency structure. We post-process U to enforce this constraint. Here we low-pass filter it with a median filter to get \hat{U} . The size of the median filter is chosen larger than a neuron size. Then the background is estimated with

$$\hat{B} = \hat{W}X + \hat{U}\hat{V}.$$

6.5 Iterative Matrix Updates and Manual intervention

Empirically after the initialization of \hat{A}, \hat{C} and approximating \hat{B} with model (3), the results are very close to the optimal solutions. But we can still make the parameter estimations better by iteratively updating model parameters. There are several things we can do: (1) deconvolve the temporal components in C to get denoised calcium traces, (2) delete false positive neurons, (3) pick neurons from the residual $Y - \hat{A}\hat{C} - \hat{B}$, and (4) merge neurons that were inappropriately split into several components. All these operations can lead to better extraction of cellular signals.

Each time when we update \hat{B} , we run the same procedure as section 6.4 again. We can adaptively change the B-spline basis and rank of UV to get better approximation. For example, when we see some trend in cellular signals, we can use spline basis with more knots to explain this trend in the background. Sometimes the background corrected data is still blurry because we do not remove the background cleanly. In this case, we can increase the rank to UV term in background to explain it.

To update \hat{A} and \hat{C} , we keep the background \hat{B} unchanged, i.e., we fit the model $\tilde{Y} = Y - \hat{B} = A \cdot C$. This can be done using the same approaches described in Pnevmatikakis et al. (2016) and we need to make changes by removing the background term (See Section 6.6).

Our method can also allow users verify the extracted cells visually and delete those low-quality neurons. The spatiotemporal activity of these deleted neurons will be absorbed by the background \hat{B} or other neurons. The signal qualities of nearby neurons might be improved. To add a neuron from the residual $Y - \hat{A}\hat{C} - \hat{B}$, we first select one pixel \mathbf{x}^* (usually the one with the maximum residual) and then run a rank-1 NMF in a small window centered at \mathbf{x}^* to get its spatial and temporal components. We can also manually or automatically select \mathbf{x}^* . Although these steps are simple, they showed great helps in speeding up the model fitting procedure. As a comparison, PCA-ICA method has no manual intervention steps. Removing false positive neurons could not improve signal extraction of other neurons.

6.6 Update \hat{A}, \hat{C}

After subtracting the background from the raw data, we can optimize A and C by fitting the model

$$\tilde{Y} = Y - \hat{B} = A \cdot C + E. \quad (19)$$

This is the same CNMF problem as proposed by Pnevmatikakis et al. (2016). The trivial difference is that Eq. (19) has no background term. We can use the same optimization procedure to estimate A, C . Here we rewrite their approaches for this optimization approach. Briefly they iteratively update A and C by solving two optimization problems. (1) Given the estimates of $C^{(k-1)}$ in previously iterations, $A^{(k)}$ can be updated by solving the following convex problem

$$\begin{aligned} \min_A \quad & \|A\|_1, \\ \text{s.t.} \quad & A \geq 0 \\ & \|\tilde{Y}(i, :) - A(i, :)C^{(k-1)}\| \leq \sigma_i\sqrt{T}, \text{ for all } i = 1 \cdots d, \end{aligned} \quad (20)$$

where σ_i is the standard deviation of the Gaussian noise for each pixel i . (2) Once we update A^k , we update $C^{(k)}$ column by column. To update the j th column, we first form the quantity

$$(\mathbf{y}_j^{(k)})^T = \frac{\mathbf{a}_j^{(k)}}{\|\mathbf{a}_j^{(k)}\|_2^2} (Y - [\mathbf{a}_1^{(k)}, \dots, \mathbf{a}_{j-1}^{(k)}, \mathbf{a}_{j+1}^{(k)}, \dots, \mathbf{a}_K^{(k)}][\mathbf{c}_1^{(k)}, \dots, \mathbf{c}_{j-1}^{(k)}, \mathbf{c}_{j+1}^{(k-1)}, \dots, \mathbf{c}_K^{(k-1)}]^T), \quad (21)$$

and then apply any deconvolution method of choice to $\mathbf{y}_j^{(k)}$ to obtain $\mathbf{c}^{(k)}$. We usually use the noise-constrained deconvolution method used in Pnevmatikakis et al. (2016).

Removing the spatial sparsity constraint and the temporal dynamics can significantly reduces the computation time and the results are close to the optimal solution. In this case, Eq. (19) is a plain NMF problem with some locality constrains. Friedrich et al. (2015) adapted the Hierarchical Alternating Least Squares (HALS) method (Cichocki et al. (2007)) algorithm to solve it with fast speed. In our implementations, we frequently use the HALS algorithm to get convergent results before running the full CNMF approaches.

6.7 Speed and scalability

Our method is very fast in analyzing data. In the example of the simulated data (256×256 pixels, 3000 frames), our naive MATLAB implementation took ~ 2 minutes to initialize 179 neurons out of 200 on a single desktop. Fitting the background model given \hat{A} , \hat{C} requires ~ 3 seconds. The manual interventions of adding/deleting neurons only need few clicks and they can be processed in real time. The results of our initialization step are very close the final solutions, so we only need $1 \sim 2$ CNMF iterations to update model parameters. The performances of those algorithms used for solving CNMF have been reported in Pnevmatikakis et al. (2016) and Friedrich et al. (2015).

Our implementations can be easily optimized to be faster. In the initialization step, spatial filtering and calculation of the local correlation images are the only computation-intensive parts in the processing of huge data sets. These computations themselves are very classical matrix operations and utilizing GPU can significantly make it faster. Since the initialization of each neuron is only dependent on a very small window, the whole initialization step can be easily processed in parallel by segmenting the optical field into multiple small patches. We can also use distributed computing to process the data patch by patch. Fitting the background model requires two steps: (1) the first step is approximating the baseline and slow trends. Since all pixels are independent, we can easily run it in parallel without effort; (2) the second step is basically SVD and there are plenty of existing algorithms or packages to deal with this problem for extremely large datasets. In summary, all the algorithm proposed in this paper has no scalability issues and can be easily scaled for processing any large-scale datasets.

6.8 Example neurons extracted by two methods from simulated data

We randomly picked one neurons that has been detected from the simulated data by both approaches. The extracted spatial and temporal components are shown in Figure 5.

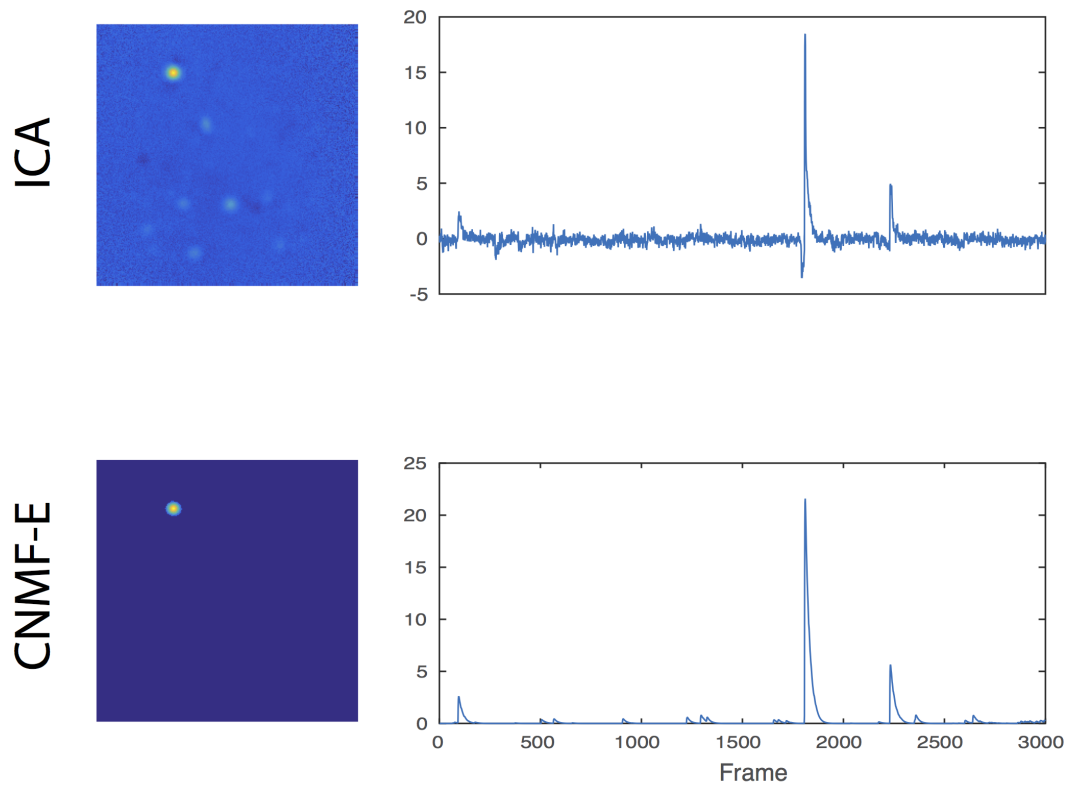


Figure 5: Spatial and temporal components of an example neuron extracted by two methods. Top row: spatial (left) and temporal component of the neuron detected by PCA-ICA. Bottom row: same as top, but it is extracted using our CNMF-E method.